Bulgarian Chemical Communications, Volume 55, Issue 3 (pp. 349-366) 2023 DOI: 10.34049/bcc.55.3.SIMNS05

Analytical modeling of stresses and strains in layered nanocomposite structures - opportunities and challenges

T. St. Petrova

Institute of Chemical Engineering, Bulgarian Academy of Sciences,
Laboratory of transfer processes in multiphase media
Acad. Georgi Bonchev Str., Bl. 103, 1113 Sofia, Bulgaria

Received: July 15, 2023; Accepted: July 31, 2023

This review aims to analyze and summarize the achievements to date, including some authors' results, in the field of analytical modeling of stresses and strains in layered nanocomposite structures, as well as the conditions under which delamination is observed in such structures. The work is organized as follows: Section 1: Brief review on papers for analytical modeling of nanocomposites (2000-2023): Section 2: Examples of analytical solutions applications to nanocomposites, Section 3: 2D analytical solutions for nanocomposites, and Conclusions.

Keywords: nanocomposites, modeling, analytical solution, stress, strain, delamination

BRIEF REVIEW ON PAPERS ABOUT ANALYTICAL MODELING OF NANOCOMPOSITES

During the last two decades a boom in publications - 193,409 publications selected from Web of Science Core Collection, dedicated to nanocomposites [1] (Fig. 1 (a)) has been seen. It can easily be verified that the largest share is occupied by the works that are mainly experimental and investigate the methods of synthesis of new, mainly polymer nanocomposites. A significant part is devoted to the study of their properties and characteristics (mechanical, optical, electrical and thermal conductivity, etc.). Another reference shows that only 392 out of 16,152 articles include modeling in addition to the experiment [2]. Given the increasingly wide application of nanocomposites in various industrial areas, the number of publications concerning modeling of the behavior of nanocomposites is also increasing - 21,776 according to Web of Science, 570 of which are review articles [3]. In most cases, commercial software products such as ANSYS, Abaqus, COSMOS, etc., are used in the modeling of nanocomposites, as complex geometries can be simulated under different types of loads on the nanocomposite; the disadvantages of this type of modeling are the time for mesh preparation and execution, sometimes the convergence of the chosen numerical method in the software; modeling a so-called "jump" in any of the sought-after quantities in a given cell/s of the mesh also creates a problem. From a total of 1,326 published articles matching the keywords “nanocomposites” and “finite element modeling” [4], 27 are review articles.

In contrast to numerical methods, analytical methods for obtaining solutions for stresses, strains and other characteristics in nanocomposites are much faster, easier and convenient to use. Their disadvantages are usually the low dimensionality of the solutions, as well as the simplification of the geometry of the considered nanocomposite and the types of loads.

As far as the author’s of the present work knowledge, there is no published review specifically dedicated to analytical methods for stress/strain modeling in nanocomposite structures, especially those in which the nanomaterial is considered as a separate layer. Given the rapid pace of research in the field and the ever-widening application of nanocomposites in industry, such a summary, accompanied by relevant analysis, would be helpful in future applications of layered nanocomposite structures, especially under specific loads.

A search was made in the available literature sources on the internet with keywords “analytical solution+nanocomposite” and “shear-lag+nanocomposites”. The result after 2004 to the present (by year) is graphically displayed in Fig. 1 (b).

* To whom all correspondence should be sent:
E-mail: t.petrova@iche.bas.bg

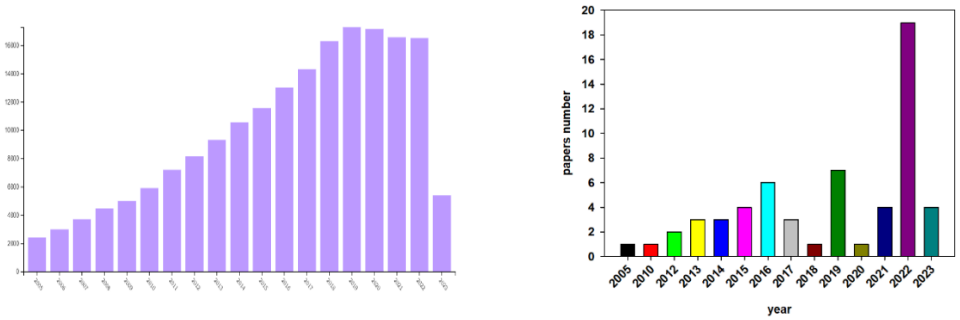

(a) (b)

Fig. 1. Number of articles found by keywords: (a) "nanocomposites", (b) "analytical solution+nanocomposites+shear-lag" during 2005-2023.

In Fig. 1 (b) the articles with results of the author of the present work (co-authored with colleagues) during the considered period are also included. From the figure it can be seen that the interest in this type of modeling systematically increased from the discovery of graphene until 2016, followed by a slight decline and the interest resumed again in the last 4-5 years. Along with graphene and the created nanocomposite structures based on graphene, whose applications are numerous and in various fields such as electronics, medicine, automotive, construction, energy, optics, etc., new 2D nanomaterials are also entering the scene - such as black phosphorus (2014), borophene (2015), MoS_2, WS_2, as well as hybrid combinations thereof like graphene/MoS_2 [5], which have yet to be extensively studied and modeled.

The classification of the types of analytical models covered in the reference can be done in several ways. If they are grouped by the dimensionality of the model, one-dimensional, two-dimensional and three-dimensional models can be distinguished. If they are grouped according to the applicability in different zones –elastic and plastic for changes in stresses and deformations - the models can be divided into linear-elastic and cohesive (plastic).

According to the dimensionality classification of the models covered in the reference, one-dimensional analytical models occupy a major share, and they are also those that refer to modeling primarily in the field of elasticity. A previous publication asset with the participation of the author of the present work contributes to this by using analytical one-dimensional model solutions to describe the behavior of two-layer composites subjected to static/dynamic loads under conditions of varying temperature, humidity and electric field [6-17]. Especially for nanocomposites, the developments with the author's participation cover one-dimensional solutions of a cohesion model for statically loaded graphene nanocomposites [13, 17] , as well as two-dimensional solutions obtained by the 2D stress-function variational method [18-24] for statically loaded nanocomposites incorporating graphene, WS_2, MoS_2 to different polymer matrices. The obtained solutions were studied by parametric analysis regarding the influence of different factors on delamination in the different types of composites and nanocomposites.

The models that give an analytical solution for higher dimensionality and/or outside the elastic region are very few, which is explainable due to the complexity in the formulation of the boundary value problems and in the computations in deriving the solutions, for example [25-28]. With the exception of [29], no other publications were found offering analytical solutions for the stresses/strains in nanocomposites under combined (mechanical and temperature) loading. An example of the joint use of analytical and/or numerical solutions for more than 1D in elastodynamics can be seen in [30-33].

In the present review, the emphasis is placed on the one- and two-dimensional analytical solutions derived for the stresses and strains in statically loaded nanocomposites. In the following sections, various examples of the available analytical models – 1D and 2D, in both the elastic and cohesive domains – will be reviewed and discussed.

EXAMPLES OF ANALYTICAL SOLUTIONS APPLIED TO NANOCOMPOSITES

The most common used one-dimensional and linear elastic model for both composite and nanocomposite structures is the so-called shear-lag model or method. Its first appearance in the literature was the work of Volkersen [34], who gave an analytical description of the stress transfer σ in a joint-type structure (single-lap joint) loaded on both sides as follows (Fig. 2).

Here, the main idea is that the connecting adhesion layer serves to transfer the load to the individual parts (arms) of the structure, and this

happens at the expense of the shear stresses τ, which distribute the load along the length of the arm connecting part *l* (Fig. 2).

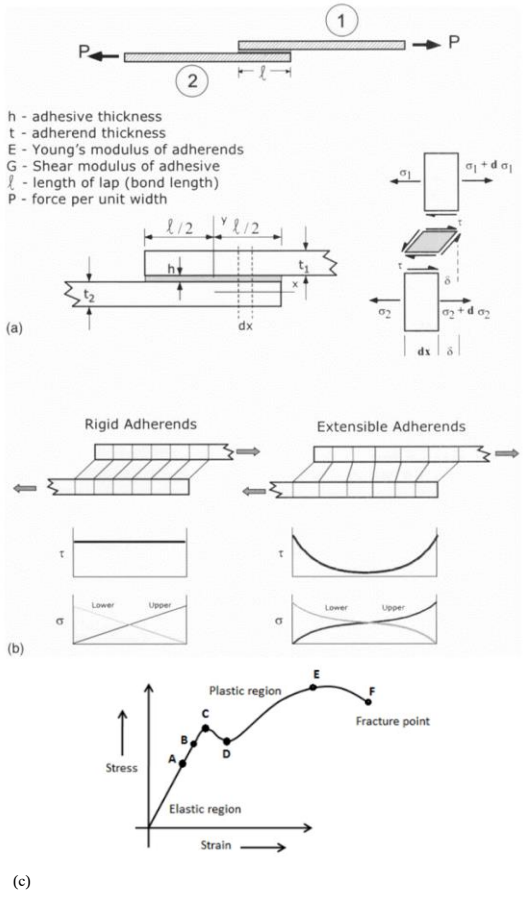

Fig. 2. Illustrative scheme of (a, b) Volkersen's shear-lag model, and (c) the stress-strain diagram [35].

In the scheme of Fig. 2 (a) and (b), it is graphically shown how the predictions of this model look analytically for the stress σ in the two arms of the structure, as well as the interfacial shear stress τ in the cases of materials with different flexibility. Volkersen offers the following analytical solution for the interphase shear stress τ for the joint structure (Fig. 2):

$$\tau(x) = \frac{P\omega}{2\sinh(\omega l/2)}\cosh\omega l + \\ + \frac{P\omega}{2\cosh(\omega l/2)}\left(\frac{E_2t_2 - E_1t_1}{E_1t_1 + E_2t_2}\right)\sinh\omega l \qquad (1)$$

where $\omega = \sqrt{\frac{G}{h}\left(\frac{E_1t_1 + E_2t_2}{E_1t_1E_2t_2}\right)}$

As can be seen, the one-dimensional analytical solution (1) depends only on x, but it also depends nonlinearly on the material characteristics of the structure - Young's modulus *E*, the shear modulus *G*, and also on the geometry of the structure - the thicknesses of the two arms t_1 , t_2 and the connecting part *h*, the length of the connecting (total) part *l*, as well as on the magnitude of the applied force *P*. This solution is derived under specific assumptions – neglecting torsion and bending, as well as normal stresses in the structure, also the effects of shrinkage due to different values of Poisson's number, as well as assuming perfect fit in *l* and linear-elastic properties for the materials in the structure. Despite the idealized formulation, this solution has its place in hundreds of publications and has been successfully validated with other models and, most notably, with experimental data in the elastic domain of applied loads [35].

Later, Cox [36], based on Volkersen's solution, revised and derived the shear-lag model and, accordingly, an analytical solution for σ and τ for fiber-matrix composite structures (composite materials containing threads or fibers, with in order to increase their resistance and strength). From Fig. 3 it can be seen that the solutions for σ and τ again depend on the applied external deformation ε_1, on the material properties of the thread and the matrix (substrate) E_f, G_m, as well as on the geometry of the object – length *L*, radius of the thread *a* and the substrate *R* (a cylindrical representative volume of the composite was considered), the thread size ratio $s=L/a$. This model obeys the same assumptions as the previous one and has been used just as widely, especially in composite structures [35]. After the emergence of nanocomposites with embedded nano-threads/fibers, especially the embedding of carbon nano-tubes in various matrices, we can trace the use of the Cox model in the following several works [37-40]. In [37], Fig. 4, left, the solutions for the stresses σ and τ are in cylindrical coordinates and in exponents, with respect to the carbon nanotube length (along the z-axis), which is mathematically similar to Cox (Fig. 3), since as hyperbolic sines and cosines are expressed with exponents, which is also confirmed by the graphical representation of σ and τ in both figures. In the work [38], to the analytical solution for the interfacial shear stress $\tau=\mu(q_0-q_1+q_2)$ the effects of additional residual stresses q_0, q_1 and q_2, arising respectively due to the different coefficients of thermal expansion of the two materials, are added, from the difference in Poisson numbers, and from the action of cohesive Van der Waals (WdW) forces (Fig. 4, right). In both examples, the solutions contain the geometric and material characteristics of the materials making up the nanocomposites, as well as the external load, and in [38] other characteristics such as thermal expansion coefficients, Poisson's ratios and cohesive forces are also considered. It is worth to note, that in [38] an external influence other than mechanical is

considered and accounted for in the model solution. The use of a simpler basic model to which analytical solutions can be added/ quantifying additional effects is a well-known mathematical approach that gives great results, but is unfortunately too rarely used, mostly due to difficulties in finding data on additional effects and quantifying them. Kundalwal *et al.* [39] presented a three-phase (three types of materials) shear-lag model for a polyamide nanocomposite containing a carbon filament to which carbon nanotubes were attached in a brush-like manner; the nanocomposite is subjected to a three-dimensional static load (Fig. 5, left). Here the solutions for the stresses σ and τ are again expressed as a combination of hyperbolic sines and cosines and integration constants. In the same work, a comparison of the results obtained by the authors with results of the finite element method (FEM) is made; the agreement is more than good, confirming the use of analytical solutions in modeling even for three-phase nanotube/matrix nanocomposites.

In the publication of Hu *et al*. [40], one can again observe the addition of additional modeling of the interfacial shear stress τ to the basic shear-lag solutions. In particular, the interphase boundary is modeled by a spring layer model with its own stiffness coefficient *K*, which is reflected in the coefficient α of the exponents in the solutions (Fig. 5, right).

In practice, this means that the interphase shear stress does not transmit the transfer of the applied external stress directly and proportionally, but is limited by the value of the coefficient *K*.

After the discovery of the stable two-dimensional form of graphene (2004, although its existence is known since 1930), attempts were made to model the behavior of graphene nanocomposites, where the nanomaterial is a 2D two-dimensional lattice/flake with an atomic thickness of 0.35 nm, incorporated or deposited in/on other material/s. The beginning of the modeling of graphene and other nanocomposites by the application of the shear-lag model to analytically describe the behavior of σ and τ was laid with the pioneering works of Nobel Price Laureates Novoselov and Geim. In their works [41, 42], shear-lag was applied for the first time to a Graphene/SU-8/PMMA nanocomposite subjected to static axial external deformation (Fig. 6).

The solutions for the interfacial tension τ and for the strain in the graphene layer e_f are again described by hyperbolic sines and cosines for external loading up to 0.4% successfully with the shear-lag model. At an external strain of 0.6%, however, the graphene begins to wrinkle, that is, the behavior becomes non-linear and the model cannot correctly describe the experimental data.

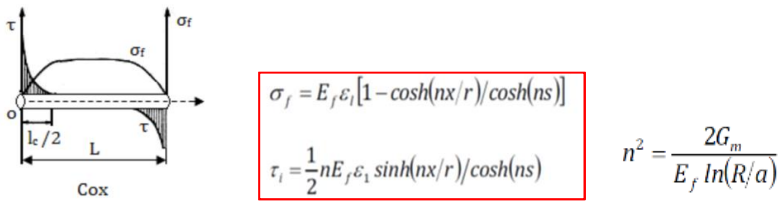

Fig. 3. Cox model and solution for fiber/filament-incorporated composites [35].

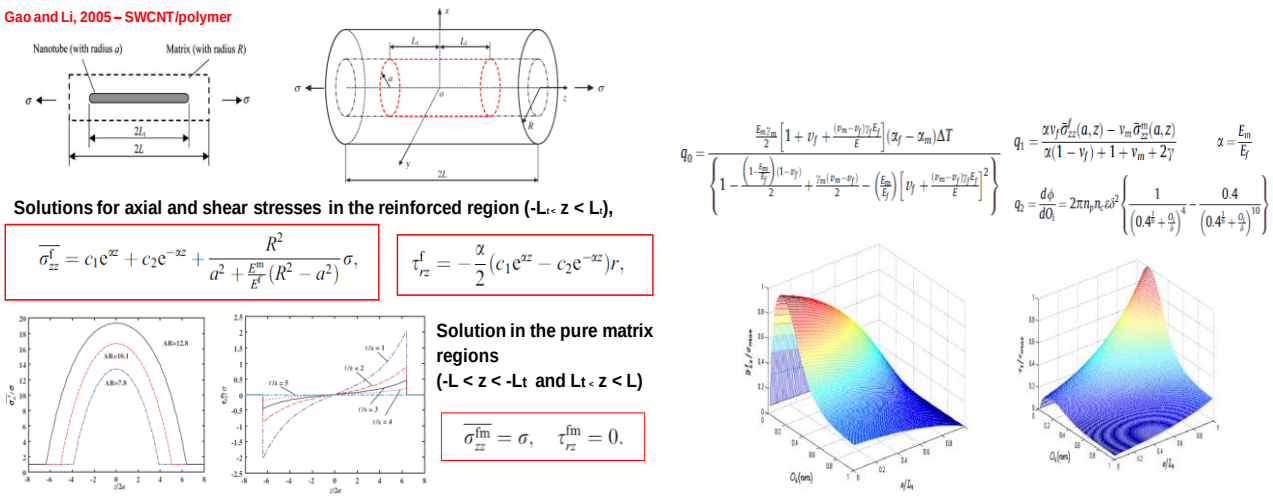

Fig. 4. Application of the Cox model to fiber nanocomposites: left [37], right [38].

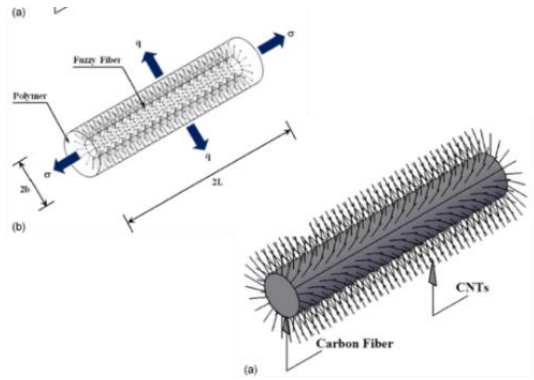

$$\tau_1 = -\frac{a}{2}[A_{36}\alpha\cosh(\alpha x) + A_{37}\alpha\sinh(\alpha x) + A_{38}\beta\cosh(\beta x) + A_{39}\beta\sinh(\beta x)]$$

$$\bar{\sigma}_x^f = A_{36}\sinh(\alpha x) + A_{37}\cosh(\alpha x) + A_{38}\sinh(\beta x) + A_{39}\cosh(\beta x) + (A_{33}/A_{32})\sigma - (A_{34}/A_{32})q - (A_{35}/A_{32})\tau \quad (38)$$

$$\left(w_i^m - w_i^f\right)K = \tau_i^f,$$

$$\overline{\sigma_{zz}^f} = c_1 e^{\alpha z} + c_2 e^{-\alpha z} + \frac{R^2}{a^2 + \left(R^2 - a^2\right)\frac{E^m}{E^f}}\sigma,$$

$$\tau_{rz}^f = -\frac{\alpha}{2} r\left(c_1 e^{\alpha z} - c_2 e^{-\alpha z}\right),$$

$$\sigma_{zz}^m = \frac{R^2}{R^2 + a^2\left(\frac{E^f}{E^m} - 1\right)}\sigma + \left(c_1 e^{\alpha z} + c_2 e^{-\alpha z}\right) \times \left\{\left[1 - \beta\left(R^2 - a^2\right)\right]\left(\frac{E^m}{E^f} - \frac{aE^m}{2K}\alpha^2\right) - \beta a^2\right\}$$

α depends now on the parameter K – interface spring stiffness parameter

Fig. 5. Application of the Cox model to fiber nanocomposites: left [39], right [40].

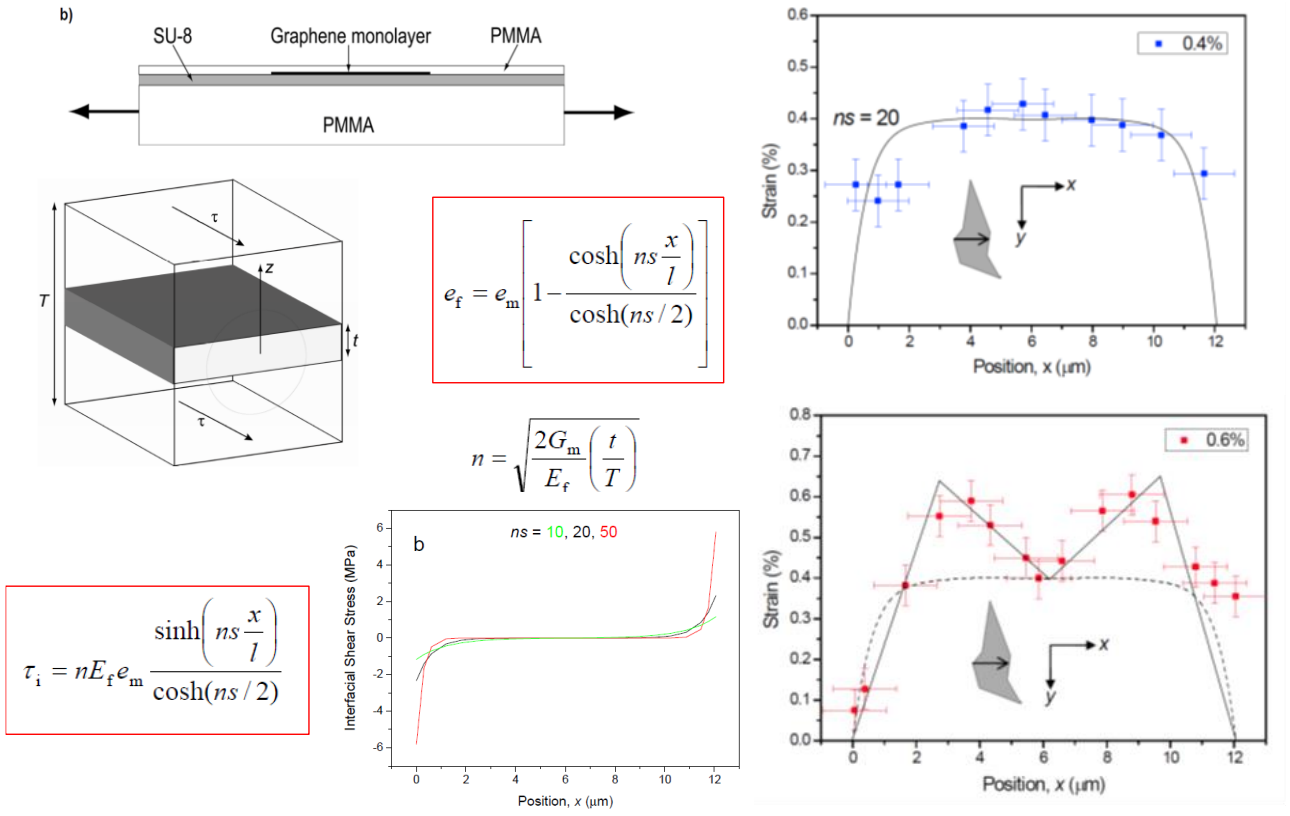

$$e_f = e_m\left[1 - \frac{\cosh\left(ns\frac{x}{l}\right)}{\cosh(ns/2)}\right]$$

$$n = \sqrt{\frac{2G_m}{E_f}\left(\frac{t}{T}\right)}$$

$$\tau_i = nE_f e_m \frac{\sinh\left(ns\frac{x}{l}\right)}{\cosh(ns/2)}$$

Fig. 6. Illustrative scheme of σ and τ solutions and nanocomposite–shear-lag [41,42].

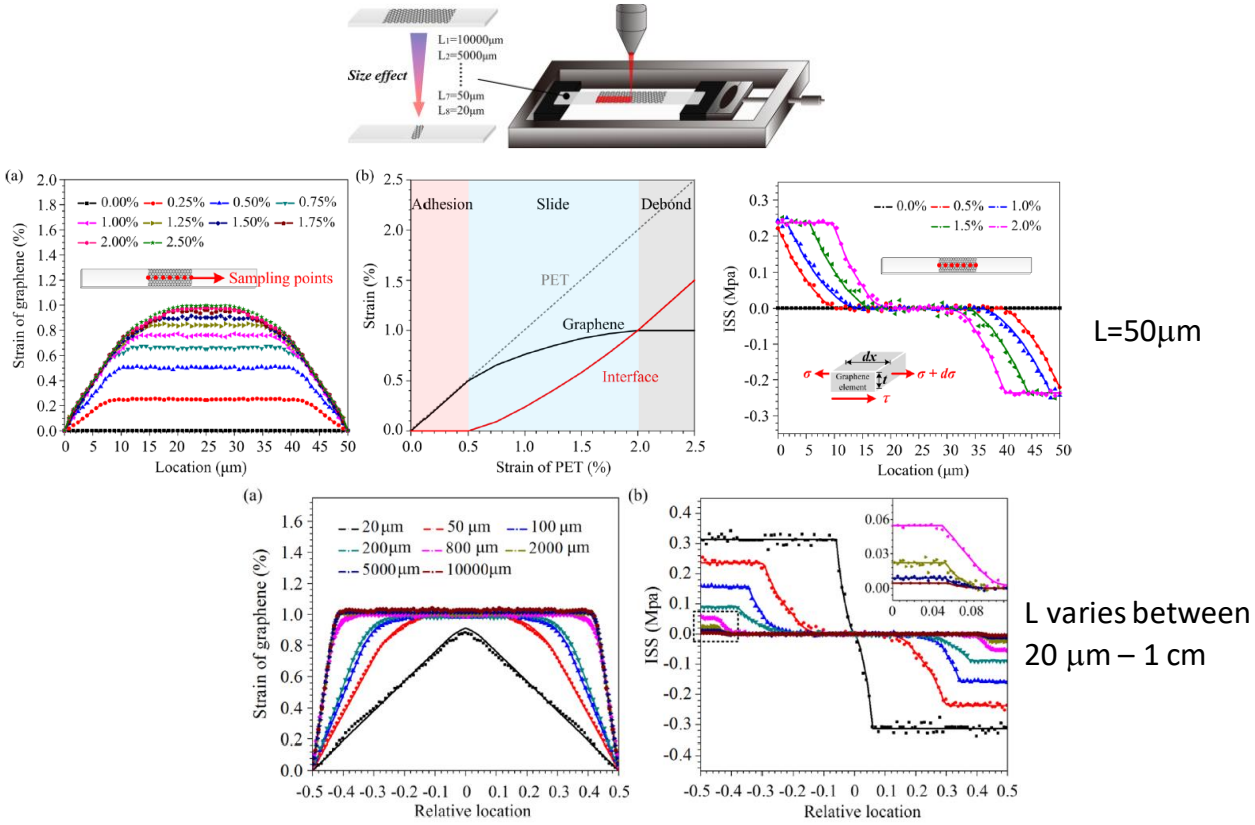

Fig. 7. Illustrative scheme of ε and τ solutions and graphics - shear-lag [43].

Shortly thereafter, Xu *et al*. [43] investigated the influence of the length of the graphene flake/layer on the value of the interfacial shear stress and on the strain in the layer, again with shear-lag (Fig. 7). They found with parametric analysis that the length of the graphene layer significantly affects the stress transfer between the layers of the nanocomposite and specifically, τ and the strain in graphene ε. As the loading in the PET substrate increases, the strain ε in the graphene linearly increases until reaching a sliding mode and a retention plateau, after which exfoliation of the graphene flake/layer follows. As the length of the graphene flake/layer increases from 20 to 10000 μm, the interfacial tension τ decreases until complete exfoliation occurs. The interfacial mechanical properties of graphene less than 20 μm long are extremely sensitive to its length, while for graphene longer than 1000 μm they are no longer size dependent. After Gong's breakthrough, more researchers are still successfully using the shear-lag model to describe the behavior of σ and τ in nanocomposites with a combination of different 2D nanomaterials and polymer matrices (PET, PMMA): tungsten disulfide WS_2 [44], hybrid nanocomposites – a combination of MoS_2 and graphene [5], boron nitride hBN [45], as well as the titanium carbide Ti_3C_2 known in the literature as Mxene [46]. An overview of the obtained results can be briefly followed in Figs. 8 ÷10. As can be seen from the figures, the solutions of the shear-lag model for the deformations in the nanomaterial layer successfully describe the experimentally measured data in the elastic region of the externally applied mechanical loads. Given the different mechanical properties of the investigated nanocomposites, and in particular, the choice of materials in the nanocomposite, the applicability limits of the model will also depend on this. It also turns out that the thickness of the nanomaterial layer is significant – for example, in [44] for the same applied external strain of 0.55%, the model solution for the strain in the WS_2 monolayer well describes the experimental data, but with several WS_2 layers this is no longer so, as a tendency to form wrinkles in the middle of the layer appears (Fig. 8, right, (d)), because of the interactions between the nanomaterial layers.

In Fig. 9 the effect of the interaction of two different nanomaterials – graphene and molybdenum disulfide – on the transfer of stress from the PET polymer layer to the upper two layers is observed. It can be seen that in sample I of Fig. 9 the transfer is 100% from polymer to MoS_2 for loadings up to 1.2%, while in sample II with two nanolayers, the transfer drops to 75% from MoS_2 to graphene even at 1% external loading; as the external load increases, the stress transfer between the layers continues to decrease. This effect, found experimentally, is due to the presence of a second

interphase layer in sample II [5]. Du *et al.* [5] confirmed their experimental observations with simple model, based on the force balance equations and superposition of solutions. In Fig. 10, top, it can be seen for the Ti_3C_2M-XENE/PMMA nanocomposite that the model deformation in the Ti_3C_2 layer matches well with the experimental data for 0.2% external loading; at 0.4%, however, more substantial differences begin to appear in the plateau region for ε [46]. When modeling the deformation in a 50-layer (17 nm) boron nitride nanocomposite hBN /PMMA (Fig. 10, bottom), the limits of the external load, up to which the model well describes the experiment, are even lower - up to 0.15% external load [45].

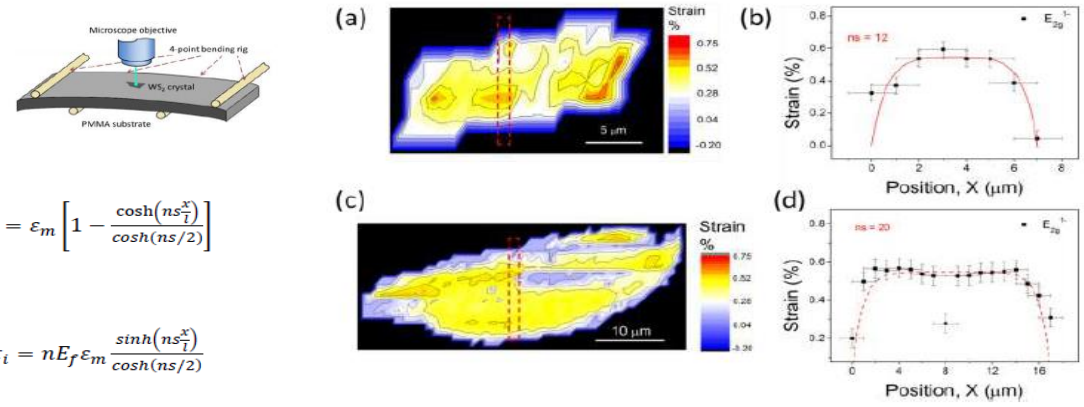

Fig. 8. Illustrative scheme of ε and τ solutions and graphics - shear-lag [44].

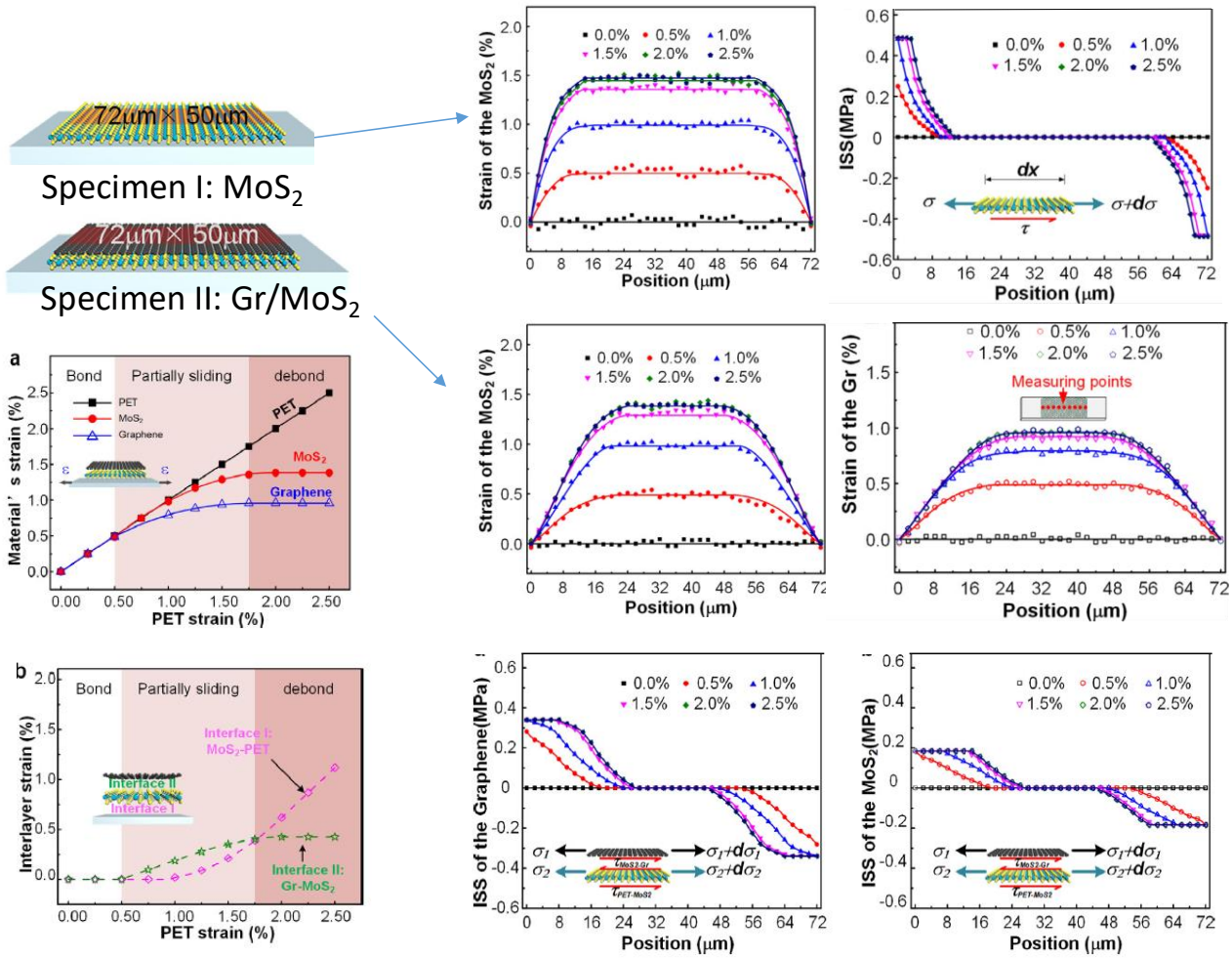

Fig. 9. Illustrative scheme of ε and τ solutions and graphics - shear-lag [5].

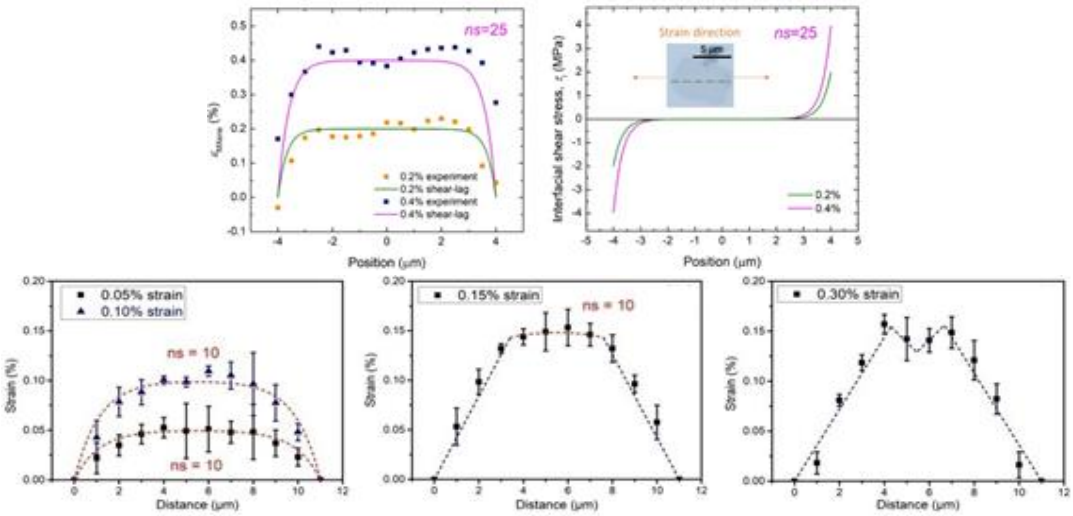

Fig. 10. Illustrative scheme of ε and τ solutions and graphics - shear-lag, (top - [46], bottom – [45]).

As mentioned, the shear-lag model and its variations considered so far give solutions valid in the elastic region of external loads. When loading above this zone (up to 0.2 ÷ 0.4%, depends on the material) a different behavior is observed - the materials begin to slip and slide and the relationship between stresses and deformations is no longer linear (Fig. 2 (c), stress-strain diagram [47]). After this yield point, the stresses again non-linearly increase until the so-called fracture mode of the respective material/structure is reached. In order to analytically describe the stresses and strains outside the elastic zone, one-dimensional models operating in the yield zone were created. These are the so-called partial debonding model and total debonding model [48]. These models were developed to describe the stresses in fiber/matrix reinforced composites and were later used for nanocomposites [49]. In the partial debonding model, debonding is assumed to start at a distance ml/2 from the matrix ends, where m is a number between 0 and 1, and represents the dimensionless length of the debonded portion. Perfect adhesion is assumed in the central part of the thread. The stresses - axial σ_f and shear τ, are determined by equations (2), and are graphically presented in Fig. 11.

$$\sigma_f = 4\tau_i\left(\frac{l}{2}-x\right)/d, \quad \tau=\tau_i$$

$$m=\frac{E_f\varepsilon-2\frac{\tau_{deb}}{n}\coth\left(ns(1-m)\right)}{2\tau_i s} \qquad (2)$$

In the total debonding model, when the fiber is detached from the supporting matrix along its entire length, i.e., m=1, and if s is the quotient of the length and diameter of the fiber, we will have the following expressions for σ and τ , and respectively the graphs (Fig. 11):

$$\sigma_{f,\max}=2\tau_i s \qquad (3)$$

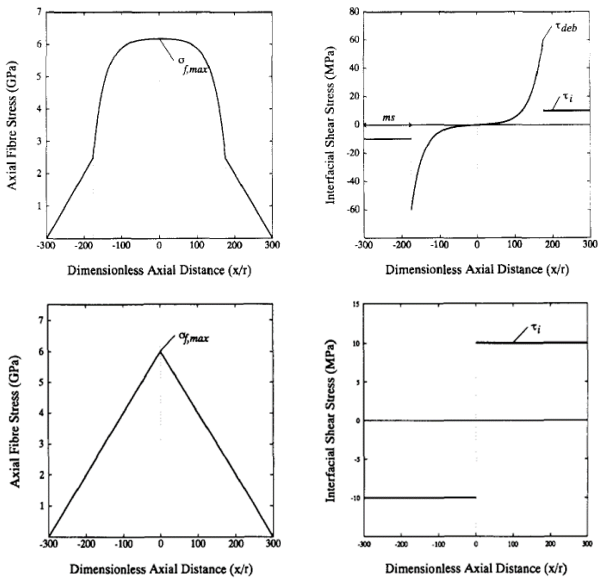

Fig. 11. Illustrative scheme of σ and τ solutions for the partial debonding (top) and total debonding models (bottom) [48].

In cases where we are between the yield and failure limits, other models are applied to predict the stresses and strains in nanocomposites - the so-called cohesive or plastic models, also nonlinear shear lag type, which also provide analytical solutions in these areas [50-54]. The next few figures illustrate the results obtained by the aforementioned researchers. Given the rather voluminous output of solutions for these models, they are presented schematically here.

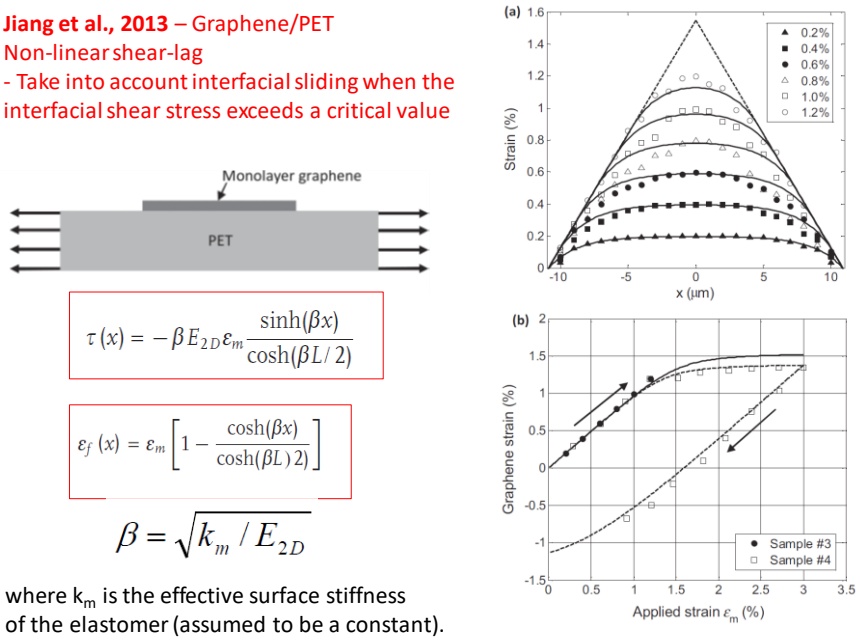

Fig. 12. Illustrative scheme of ε and τ solutions and graphics – non-linear shear-lag for graphene/PET, [50].

As can be seen from Fig. 12, the solutions for ε and τ closely resemble those of ordinary shear-lag as combinations of hyperbolic sines and cosines. The difference is in the value of the β parameter in the x argument. Here, an additional constant k_m is also included in the parameter, which represents the effective stiffness of the polymer surface. The analogous parameter *ns* in shear-lag (see Fig. 6) does not take into account this effect, and here the sliding of the interfacial boundary is also taken into account when the interfacial tension exceeds a certain critical value (for the considered nanocomposite it is at 1.2% external load). The graphs for the deformations in the graphene layer above the elastic zone are described very well by the nonlinear shear-lag at values of the external strain up to 3%. A similar result was achieved with the same nonlinear model in [51] for a graphene/cobalt nanocomposite (Fig. 13). In this work, the parameter β is again used, but in it, in addition to the k_m-like constant C, the material characteristics of the substrate (cobalt) are also included. This model accounts for the onset of sliding and, accordingly, the formation of wrinkles in graphene after a rather low level of external loading of 0.2%, due to the poor adhesion between graphene and cobalt. An application of two nonlinear models, as well as the finite element method to describe the deformations in graphene above the yield zone can be seen in the work [52] (Fig. 14). A cohesive model with shear-lag analysis was combined, and 5 behavior modes were established for the strain distribution for an external load of up to 3.3%. Applying this modeling approach allows determining important characteristics for the nanocomposite above the elastic limit such as interface stiffness, shear strength, and fracture toughness. A parametric analysis was also performed, which showed that higher interface stiffness and/or shear strength lead to higher stress transfer efficiency, while higher fracture toughness can delay debonding (delamination).

As can be seen from the graphical comparison of the solutions in Figs. 15 and 16 with the experimental data or with the FEM, the analytical solutions created to model the deformations and interfacial stresses in different types of nanocomposites outside the elastic zone do very well. As can be seen from Fig. 12, the solutions for ε and τ closely resemble those of ordinary shear-lag as combinations of hyperbolic sines and cosines. The difference is in the value of the β parameter in the x argument.

2D ANALYTICAL SOLUTIONS FOR NANOCOMPOSITES

In contrast to the variety of 1D models and analytical solutions, described in the preceding section, the 2D models offering analytical solutions for layered nanocomposite structures are counted on the fingers. There are a lot of two-dimensional analytical solutions, offered by continuum mechanics, plate theory, etc., used for describing the behavior in layered composite structures (single lap-joint, double lap-joint) [55-57] at mechanical and/or temperature loading, but not for those incorporating 2D nanoadditives as layers.

There is a critical strain level of 0.2% beyond which sliding will occur, β = 1·106 m^{-1}.

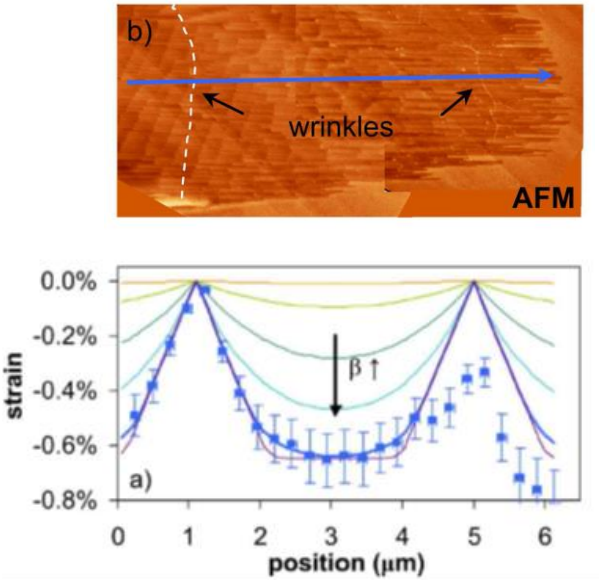

The interfacial shear strength critical τ_c of 2.2±0.3 MPa

$$\beta = \sqrt{\frac{2}{C}\frac{G_s}{t_s}}$$

G_s - the shear modulus of the substrate,
t_s - the thickness of the substrate =50 μm

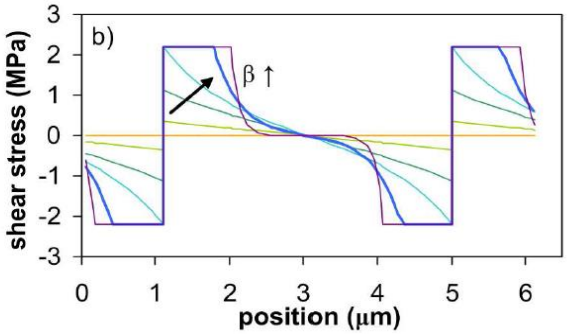

Fig. 13. Illustrative scheme of ε and τ solutions and graphics – non-linear shear-lag for graphene/cobalt [51].

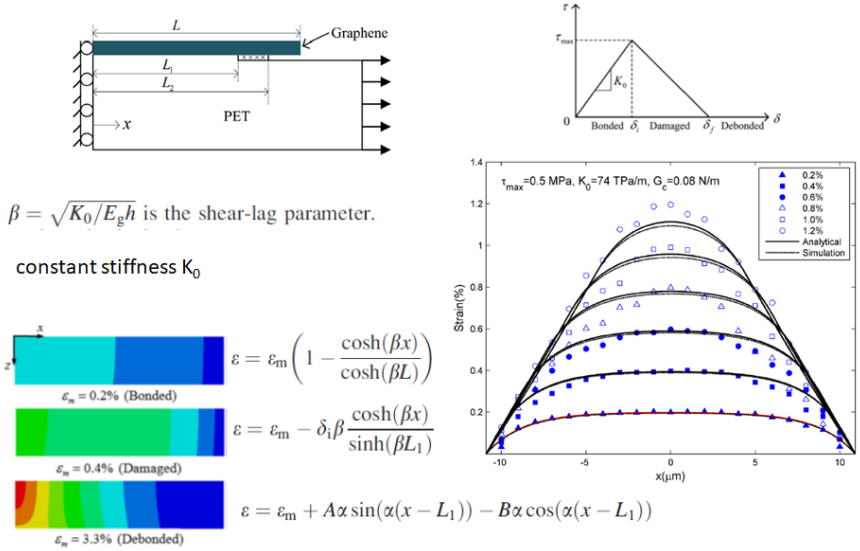

Fig. 14. Illustrative scheme of ε solutions and graphics – cohesive model, shear-lag and FEM for graphene/PET [52].

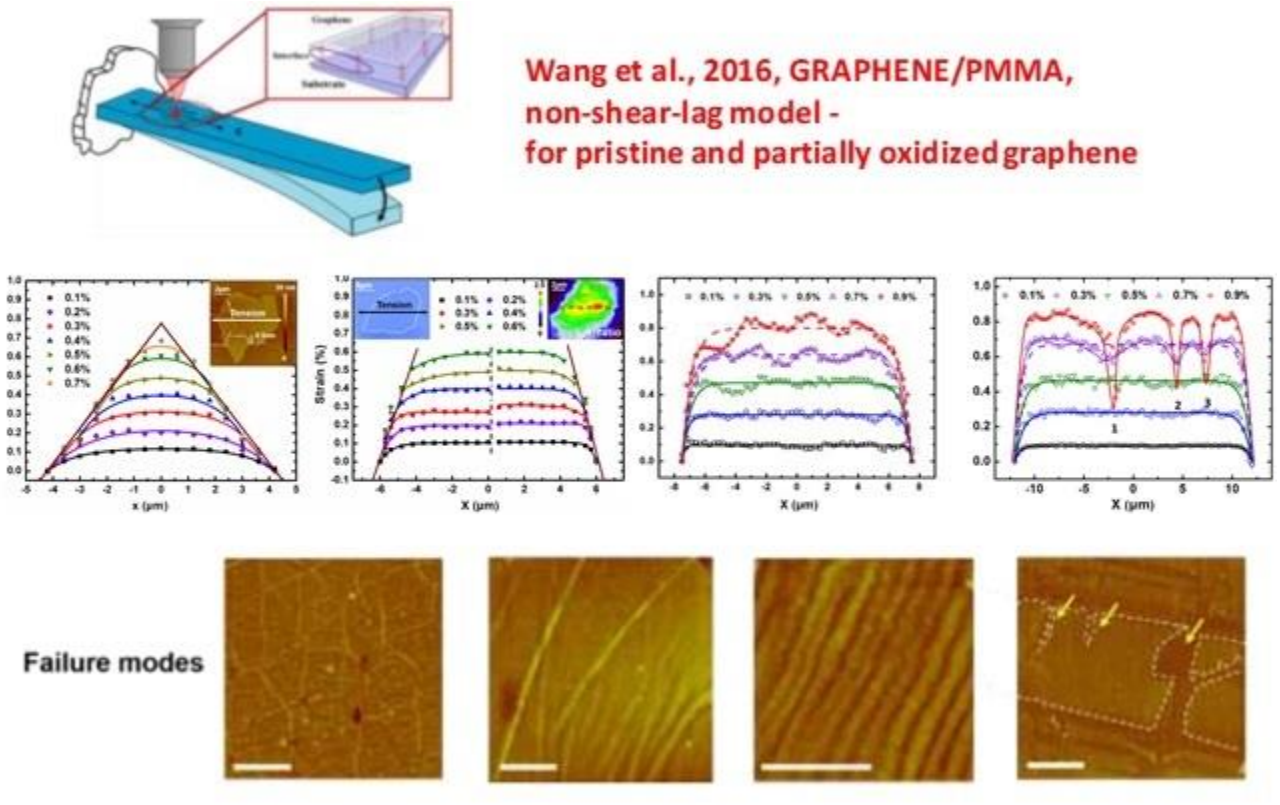

Fig. 15. Illustrative scheme of ε solutions and graphics – non-linear shear-lag for Graphene/PMMA [53].

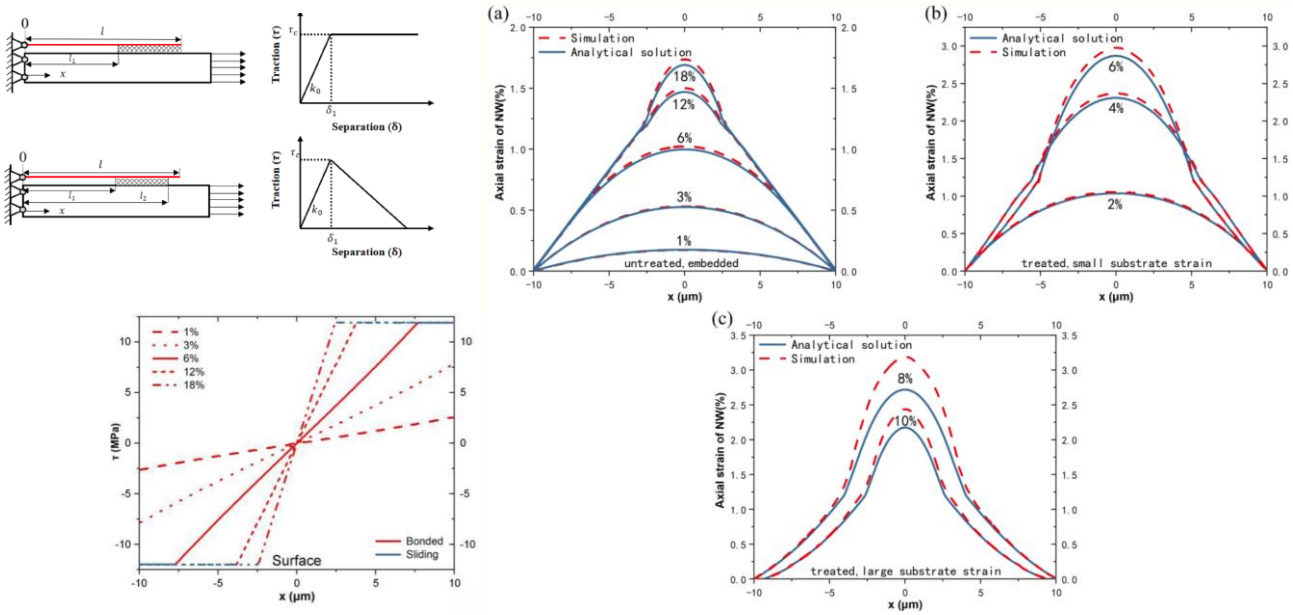

Fig. 16. Illustrative scheme of ε and τ solutions and graphics – non-linear shear-lag, bi-linear shear-lag , FEM, for elastoplastic nano-fiber AgNW/PDMS [54].

Several works were also found on so-called nano-adhesives (nanoclays), nano-additions of graphene and other 2D nanomaterials to various adhesives, in order to strengthen single-lap joint structures [58-60]. For some biological materials such as bone or nacre (generic nanocomposite structure with staggered alignment of mineral platelets in protein matrix) [61] a perturbation method was applied for analytically solving the 2D displacement and stress fields of such type of nanocomposite structure under uniaxial tension. The disadvantage of all these models is that interface layer between matrix and nano-layer are not taken into account. In 1D models like shear-lag the interface is represented as a line without considering its thickness and material properties. Meanwhile, it is proved that this interface

layer exists and should not be ignored when modeling layered nanocomposites, analytically or numerically [62-64].

From 2019, our team started to work trying to fill this gap and our contribution to the 2D analytical modeling of stresses and strain fields in layered nanocomposites with interface layer is expressed by the publications [19-24]. A detailed description of the 2D method (stress-function variational method) used to obtain analytical solutions for the two-dimensional stresses and strains in three-layer nanocomposite structures is given therein. In short, the applied method allows to obtain and solve an analytical differential equation of 4th order with respect to the unknown axial stress in the first layer (nanolayer). All other stresses in the layers are expressed by this solution/s and its derivatives. Two types of model solutions for the axial stress in the nanolayer are derived, depending on the geometry of the three-layer nanocomposite and its material properties:

$$\sigma_1 = C_1\, exp\left(\lambda_1 x\right) + C_2\, exp\left(\lambda_2 x\right) + C_3\, exp\left(\lambda_3 x\right) + C_4\, exp\left(\lambda_4 x\right) - A \tag{4}$$

$$\sigma_1 = \exp(-\alpha x)[M_1 \cos(\beta x) + M_2 \sin(\beta x)] + \exp(\alpha x).[(M_3 \cos(\beta x) + M_4 \sin(\beta x)] - A \tag{5}$$

All other stresses in the layers are expressed by one of the abovementioned solutions and its derivatives, as:

$$\begin{aligned}
&\sigma_{xx}^{(1)} = \sigma_1\left(x\right) = \sigma_1, \\
&\sigma_{yy}^{(1)} = \frac{1}{2}\left(y - y_t\right)^2 \sigma_1^{"}, \\
&\sigma_{xy}^{(1)} = \left(y_t - y\right)\sigma_1^{'} \\
&\sigma_{xx}^{(a)} \equiv 0 \\
&\sigma_{yy}^{(a)} = \left[\frac{h_1^2}{2} + h_1\left(c - y\right)\right]\sigma_1^{"}, \\
&\sigma_{xx}^{(2)} = \sigma_0 - \rho\sigma_1, \\
&\sigma_{yy}^{(2)} = \frac{-\rho}{2}\left[y^2 - y\left(y_t + h_a\right)\right]\sigma_1^{"}, \\
&\sigma_{xy}^{(2)} = \rho y\sigma_1^{'}, \quad where \quad \rho = h_1/h_2
\end{aligned} \tag{6}$$

The 2D strains in each layer are expresses by equations (4)÷(6) as:

$$\begin{aligned}
&\varepsilon_{xy}^{(i)} = \frac{\left(1+\nu^{(i)}\right)\sigma_{xy}^{(i)}}{E^{(i)}} \\
&\varepsilon_{xx}^{(i)} = \frac{\sigma_{xx}^{(i)}}{E^{(i)}} - \frac{\nu^{(i)}\sigma_{yy}^{(i)}}{E^{(i)}} \\
&\varepsilon_{yy}^{(i)} = -\frac{\nu^{(i)}\sigma_{xx}^{(i)}}{E^{(i)}} + \frac{\sigma_{yy}^{(i)}}{E^{(i)}}
\end{aligned} \tag{7}$$

For convenience, only the main results and the validation of our model solutions with literature experimental and model data will be given below. The results of the parametric analysis are also presented, which, based on the study of the sensitivity of the model solutions, makes it possible to determine the factors affecting the delamination in the investigated nanocomposite structures, given their wide application in various industrial sectors.

Validation

The validation of the model results obtained by us for the stresses and strains, with data from literature, is performed for the following nanocomposite structures: graphene/SU-8/PMMA – Gong [42], WS_2/SU-8/PMMA – Wang [44], 3-layered graphene/SU-8/PMMA - Androulidakis *et al.* [65] and Du *et al*. [5] for MoS_2/interface/PET and graphene/MoS_2/ PET. The results of the comparison of the obtained solutions can be seen below in Figs. 17 ÷21.

The validity of the proposed method and analytical solutions is only within the elastic region. It is worth mentioning that this region varies for different types of 2D nanomaterial. At 0.6% external load (Fig. 17 (b)) both model solutions - ours and the shear-lag one used in [42] cannot describe Gong's experimental data for graphene strain sufficiently accurately. The explanation for this is Gong's experimental observation that when the external load varies in the range of 0.4% to 0.7%, a creep and relaxation zone is recorded in the graphene, which is the cause of the drop (approximately in the middle of the flake, to 0.4%) in the distribution of the measured axial strain in graphene. According to Gong, it seems that the interface between the graphene and the polymer is not efficient enough and the transfer of the applied external load occurs through interfacial friction in this range. The strain in the graphene does not drop to zero in the middle of the flake, however, indicating that the flake remains unbounded. Further evidence to support this claim can be found in Polyzos *et al*. [66]. They experimentally investigated the behavior of stresses and strains in a suspended graphene flake between two PMMA layers subjected to an axial external load. It is reported that up to 0.8% external load "there is evidence that axial loading of graphene is always accompanied by the formation of orthogonal wrinkles/folds, similar to what is observed in a thin macroscopic membrane subjected to axial tension". In [66] they also emphasize that the limitations in their research method require a linear relationship between stress and strain, that is, within the elastic zone.

From Fig. 18 it is seen, that for WS_2 this depends not only on external load magnitude, but on the thickness of the +nano layer, too. As is illustrated on Fig. 19, both solutions for axial stress in WS_2 are in good agreement with shear-lag predictions, especially Case 2, may be because both shear-lag and Case 2 are expressed by hyperbolic sines and cosines. The similar dependence is observed for multi-layer graphene when external load is out of elastic range (Fig. 20). Here the main deviations are in the right end of the flakes for both external loads considered. Probably, this is due to the defect in the flake itself or to an error in measurement method in [65].

Our latter model strain predictions for hybrid nanocomposite structure with 2 interfaces (graphene/MoS_2/PET) at external load 0.5% are in good accordance with experimental data (Fig. 21 (b)). For nanocomposite sample with one interface (MoS_2/interface/PET) the coincidence is quite good (Fig. 21 (a)); probably, the existence of two interfaces in the first sample between both nanomaterials (graphene and MoS_2) and (MoS_2 and PET) did not positively influence the stress transfer efficiency in this sample.

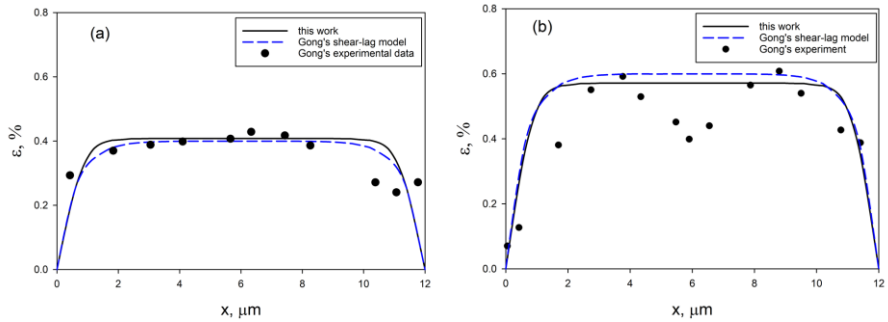

Fig. 17. Comparison of model predictions [19] for the ε in graphene with shear-lag model data and experimental data [42]; (a) at external load 0.4%, (b) – at 0.6%.

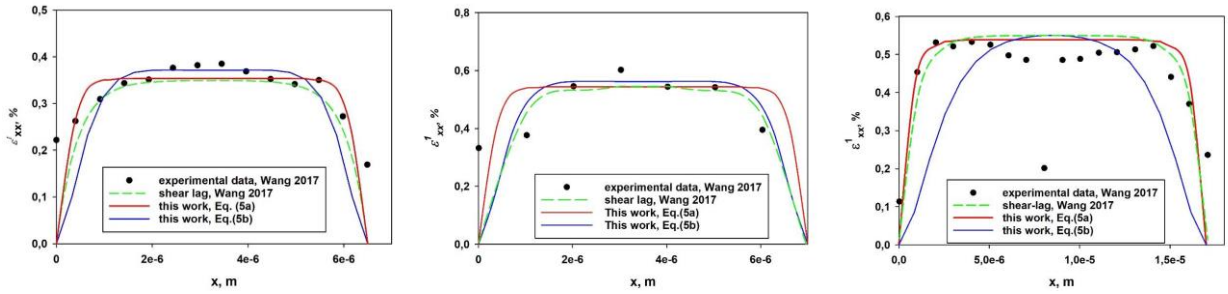

(a) (b) (c)

Fig. 18. Comparison of the two model solutions for ε in monolayer WS_2 , according to equations (4) and (5) and (7) [21], with experimental and model shear-lag data of [44] at (a) external load 0.35%, (b) same at 0.55%, (c) multilayer WS_2 at 0.55%.

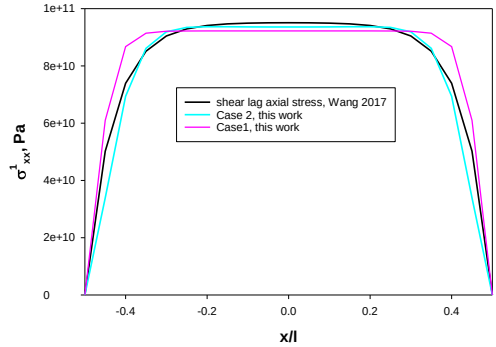

Fig. 19. Comparison of model σ solutions [24] in layer WS_2, with shear-lag model results of [44], for 0.35% external load.

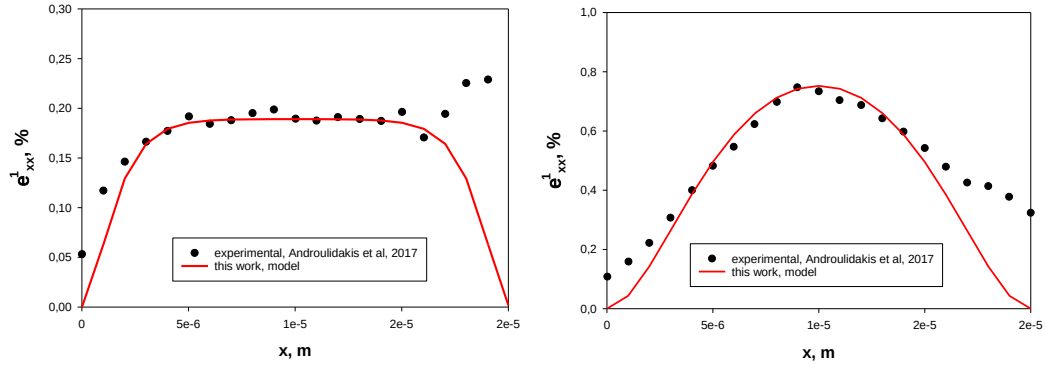

Fig. 20. Comparison of the model axial deformations [22] in 3-layer graphene with experimental data of [65], at external mechanical loading of 0.3% and 0.8 %.

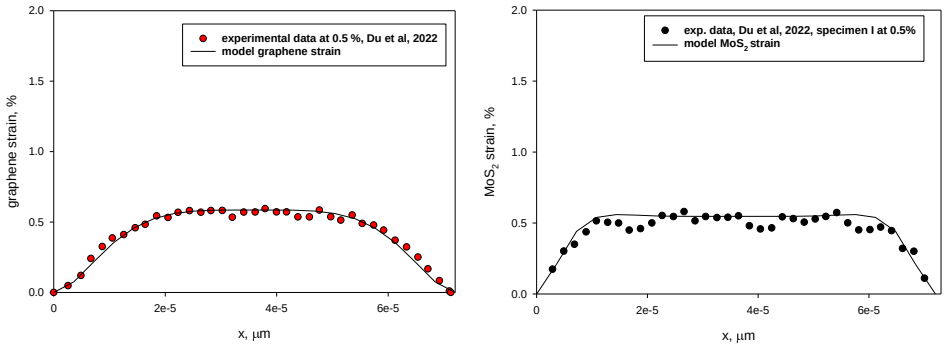

(a) (b)

Fig. 21. Comparison of the model axial ε in the graphene layer (a), and in the MoS_2 layer (b), with experimental data of [5] at an external mechanical load of 0.5%.

Our future goal is to create a two-dimensional model for a three-layer nanocomposite with two interfacial layers.

Parametric analysis

For the nanostructures considered in the previous sub-section, a parametric analysis was made to determine which factors influence the delamination in them. The criterion for delamination is that the interface shear stress (ISS) calculated by the model in the second layer exceeds the critical value of the shear stress at tension (ultimate tensile shear strength), $\sigma_{xy}^{(a)} \geq USS^{(a)}$.

For each of the structures in the previous sub-section, a parametric analysis of $\sigma_{xy}^{(a)}$ for both two solutions was performed, since each of them corresponds to a combination of different thicknesses of the layers. Thus, in addition to the influence of the length, the influence of the layer thickness on the delamination was also investigated. As can be seen from the figures below, the geometry of the nanocomposite is a significant factor in debonding.

Graphene/SU-8/PMMA

The two solutions (4) and (5) for the axial stress were considered, respectively, with the help of equation (6) the shear stress $\sigma_{xy}^{(a)}$ in the second layer was calculated, as well as the abovementioned delamination criterion. For convenience, depending on the solution used, they are referred to as Case 1 (4) and Case 2 (5) in the following text. It was found that in the thinner layers (Case 1) of considered nanocomposite graphene/SU-8/PMMA, delamination can be observed at values of the external load $\sigma_0 \geq 350MPa$, while in the thicker layers (Case 2) it occurs for $\sigma_0 \geq 750MPa$, at a fixed value of the length l (Fig. 22). As the length increases and other parameters are fixed, delamination starts at lower values of the external load (Table 1). Also, the magnitude of σ_0 affects strongly the value of the debond length. The latter one is the solution of the equation $\sigma_{xy}^{(a)}(x) = \sigma_{USS}^{(a)}$ with the ultimate shear strength of the SU-8 adhesive (USS) on the right $\tau_{cr} = \sigma_{USS}^{(a)} = 30MPa$. The delamination starts simultaneously from both ends of the structure and graphically its length corresponds to the intersection of the model $\sigma_{xy}^{(a)}$ with the critical value (red line). The obtained data

for the distance of the maximum value of $\sigma_{xy}^{(a)}$ from the edges of the layer are respectively 1.5 μm and 3.5 μm for Case 1 and Case 2 at maximum load, which values agree very well with the experimentally obtained data in [67] for the same structure – about 2 μm.

WS_2/SU-8/PMMA

For the WS_2/SU-8/PMMA nanocomposite, the parametric analysis follows the same algorithm, again using both solutions, and the results are given in Figs. 23 and 24. Results were also obtained for the delamination length at different geometries (Fig. 24). As the length of the structure increases, so does the delamination length.

Table 1

Case	l =6 μm	l = 12 μm	l = 20 μm	l = 30 μm
Case 1	$\sigma_0 \geq 2.5\times10^8$ Pa	$\sigma_0 \geq 3.5\times10^8$ Pa	$\sigma_0 \geq 8.5\times10^8$ Pa	$\sigma_0 \geq 3.3\times10^9$ Pa
Case 2	$\sigma_0 \geq 7.5\times10^8$ Pa	$\sigma_0 \geq 7.5\times10^8$ Pa	$\sigma_0 \geq 7.2\times10^8$ Pa	$\sigma_0 \geq 8\times10^8$ Pa

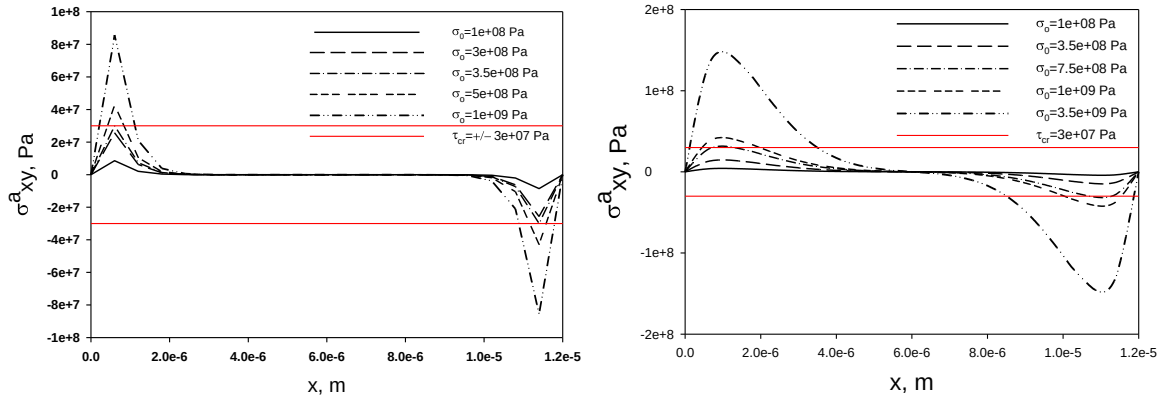

Fig. 22. Influence of the magnitude of the external load on the ISS for two different geometries (solutions) [20]; left, Case 1, right, Case 2, for monolayer graphene/SU-8/PMMA.

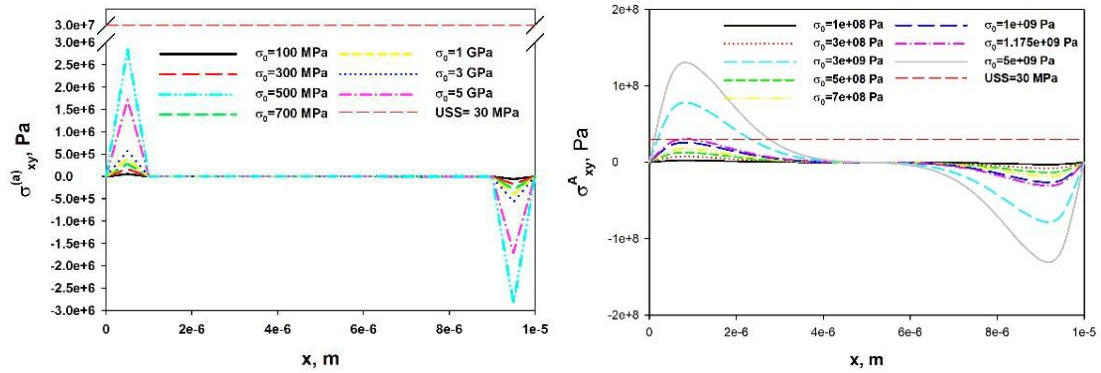

Fig. 23. Influence of the magnitude of the external load on the ISS at two different geometries (solutions) [23]; left, Case 1, right, Case 2, for the monolayer WS_2/SU-8/PMMA nanocomposite structure.

A similar result was also observed by Wang *et al.* [68] for the delamination length – 2 μm, for a WS_2/PVA nanocomposite structure.

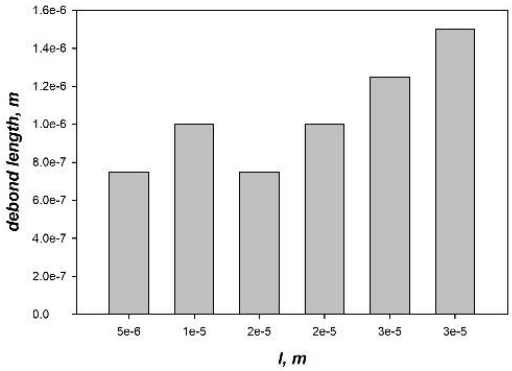

Fig. 24. Relationship between the debond length and the length *l* at a fixed load of 3 GPa, for Case 2, monolayer WS_2/SU-8/PMMA [23].

3-layered graphene/SU-8/PMMA

The main emphasis in [22] is the comparison between the model solutions for the deformations (strains) in the layers of considered 3-layered graphene/SU-8/PMMA nanocomposite, under different types of external loads, as can be seen from Fig. 25. In the case of a purely thermal effect (the red line), the deformations are nearly three times smaller than in the case of a purely mechanical effect (the black line). In the thermomechanical (green line), a superposition effect is observed in the amplitudes of the two loads, or in other words, the behavior is the same as in the mechanical load, but stronger, with the addition of the temperature effect, and this is best seen in the axial and the normal stress. Also, the effect of temperature is more clearly visible for deformations in the polymer layer than in graphene.

A similar observation is also found in the model results of Banaronei [29] obtained with finite elements. The work [29] is the first (to the best of our knowledge) to report results related to the distribution of stresses and longitudinal strains in graphene at different external temperatures. Since the simulation used in [29] is FEM, no direct quantitative comparison is possible, only a qualitative assessment.

CONCLUSIONS

After this review on the analytical models for layered nanocomposites in the literature, the following conclusions and remarks could be proposed:

✓ Analytical "shear-lag" type models give simple 1D solutions, validated by experiments and FEM, for prediction of stresses and strains in composite and nanocomposites structures, subjected generally in tension loading.

✓ Analytical models allow adding of different effects to the stresses, especially to ISS, like interface spring stiffness constant, effects of residual stresses, due to the thermal and Poisson contraction, effect of WdW forces, effect of sliding, etc., and obtain analytical solutions to describe a complex combination of external and internal factors, acting on the stress transfer in nanocomposites.

✓ The correct application of shear-lag models for matrix-fiber nanocomposites is constrained - firstly in the elastic zone only, secondly by the volume of added fibers, and also, by the fiber length and interaction between fibers. Different models are derived to cover these gaps.

✓ Partial and total debonding models, as well as non-linear shear-lag create the "bridge" between predictions of stress transfer in elastic and plastic zone (cohesive shear-lag models and FEM simulations).

✓ 2D analytical stress-function method allows deriving of 2D solutions for three-layer nanocomposite structure, subjected to mechanical (axial tension) and thermo-mechanical static loading. These solutions are successfully validated in elastic zone by experimental and shear lag data for different nanocomposite structures.

(a) (b) (c)

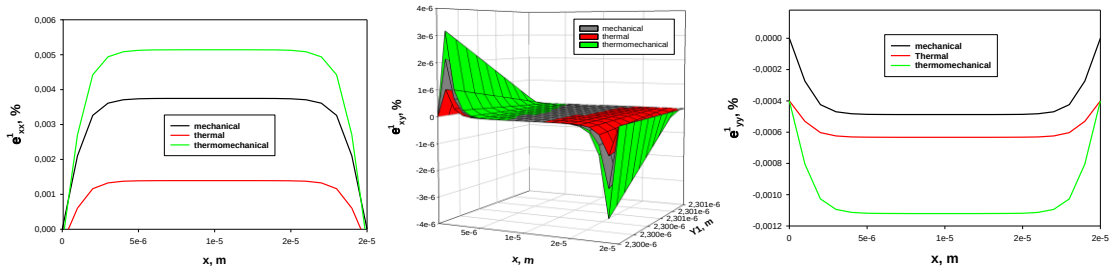

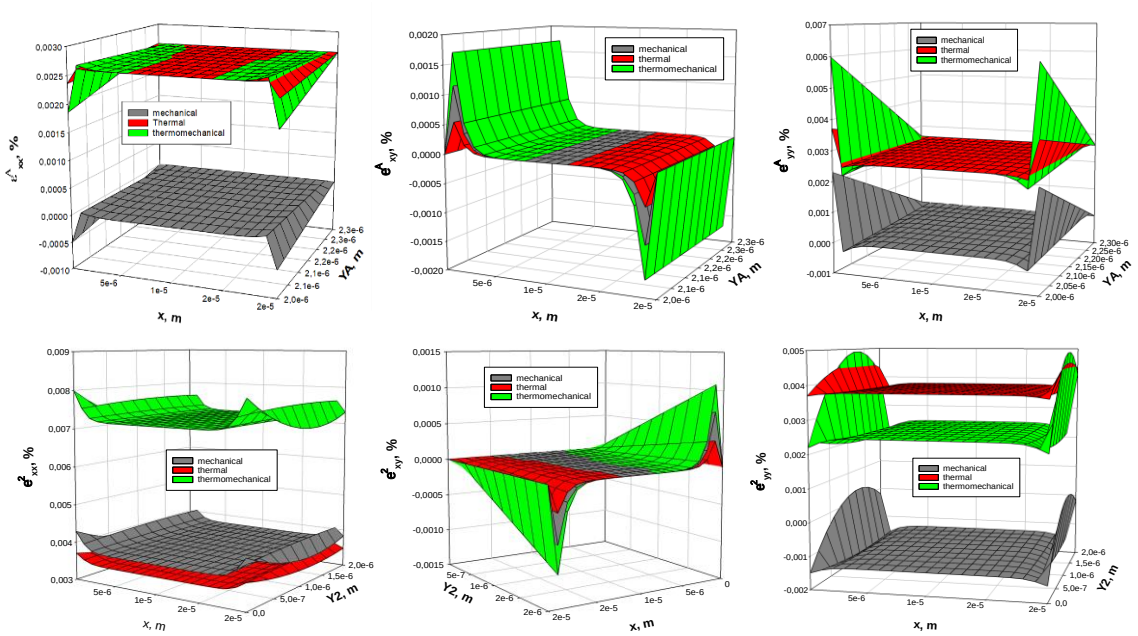

Fig. 25. Comparison of axial (a), shear (b) and peel strains (c) in graphene/SU-8/PMMA layers, under different types of loading [22].

Acknowledgement: *The author gratefully acknowledges the Bulgarian National Science Fund for its financial support via the contract for project КП-06-Н57/3/15.11.2021.*

REFERENCES

1. https://www.webofscience.com/wos/woscc/analyze-results/c956e875-4c9b-4d86-bd77-4ec87361bb63-91512fea, Assessed 26.06.2023.
2. https://www.webofscience.com/wos/woscc/summary/31c88f67-3965-4d38-8085-1e8a776b8d9c-9153a127/relevance/1, Assessed 26.06.2023.
3. https://www.webofscience.com/wos/woscc/summary/7a2f8a88-c322-4465-8e51-f594f1d9e179-9153d409/relevance/1, Assessed 26.06.2023.
4. https://www.webofscience.com/wos/woscc/summary/d8b0db8c-a5a0-4a07-9d8d-9413902b8ff1-9152f4f4/relevance/1, Assessed 26.06.2023.
5. H. Du, Y. Kang, C. Xu, T. Xue, W. Qiu, H. Xie, *Optics and Lasers in Engineering*, **149**, article 106825 (2022).
6. V. Valeva, T. Petrova, J. Ivanova, W. Becker, in: Proc. of Int. Conf. on Civil Engineering, Design and Constructions, 13 ÷ 15 September 2012, Varna, Bulgaria, 412.
7. J. Ivanova, V. Valeva, T. Petrova, W. Becker, in: Proc. of 8-th Conference on Sustainable Development of Energy, Water and Environmental Systems, September 22-27, (2013), Dubrovnik, Croatia, 0929-1.
8. J. Ivanova, V. Valeva, T. Petrova, W. Becker, *Mechanics of Advanced Materials and Structures*, **22** (10), 813 (2015).
9. J. Ivanova, V. Valeva, A. Yanakieva, T. Petrova, W. Becker, *Journal of Sustainable Development of Energy, Water and Environment Systems*, **4** (1), 23 (2016).
10. J. Ivanova, T. Petrova, E. Kirilova, W. Becker, *Engineering Transactions*, **65** (1), 97 (2017).
11. W. Becker, V. Valeva, T. Petrova, J. Ivanova, *Chemical Engineering Transactions*, **42**, 91 (2014).
12. E. Kirilova, T. Petrova, W. Becker, J. Ivanova, *ZAMM*, **97** (9), 1136 (2017).
13. E. Kirilova, T. Petrova, W. Becker, J. Ivanova, *IOP Conference Series: Materials Science and Engineering (MSE)*, **461** (1), 012029-1 (2018).
14. T. Petrova, E. Kirilova, W. Becker, J. Ivanova, *Pliska Studia Matematica*, **25**, 119 (2015).
15. T. Petrova, E. Kirilova, W. Becker, N. Vaklieva-Bancheva, J. Ivanova, *ZAMM*, **96**, 11, 1280 (2016).
16. T. Petrova, W. Becker, E. Kirilova, J. Ivanova, *CE/papers*, **1** (4), 487 (2017).
17. T. Petrova, E. Kirilova, W. Becker, J. Ivanova, J., *IOP Conference Series: Materials Science and Engineering (MSE)*, **461** (1), 012067-1 (2018).
18. E. Kirilova, T. Petrova, W. Becker, J. Ivanova, in: *2019 IEEE 14th Nanotechnology Materials and Devices Conference*, Stockholm, 27-30 October 2019.
19. T. Petrova, E. Kirilova, W. Becker, J. Ivanova, *J. Appl. Comput. Mech*., **8**(3), 1065 (2022).
20. A. Apostolov, E. Kirilova, R. Vladova, N. Vaklieva-Bancheva, Ts. Rangelov, *Chemical Engineering Transactions*, **94**, 463 (2022).
21. T. Petrova, E. Kirilova, R. Vladova, B. Boyadjiev, W. Becker, P. Dineva-Vladikova, *U. Porto Journal of Engineering*, **8** (6), 160 (2022).
22. R. K. Vladova, T. S. Petrova, E. G. Kirilova, A.G. Apostolov, B. Ch. Boyadjiev, *Bulgarian Chemical Communications*, **54** (4), 349 (2022).

23. E. Kirilova, T. Petrova, N. Vaklieva-Bancheva, R. Vladova, Ts. Rangelov, A. Apostolov, *Procedia Structural Integrity*, **43**, 282 (2023).
24. T. Petrova, E. Kirilova, W. Becker, N. Vaklieva-Bancheva, R. Vladova, P. Dineva-Vladikova, *Procedia Structural Integrity*, **43**, 83 (2023).
25. Y. Zhang, J. Zhao, Y. Jia, T. Mabrouki, Y. Gong, N. Wei, T. Rabczuk, *Composite Structures*, **104**, 261 (2013).
26. M. Amirpour, R. Das, E.I. Saavedra Flores, *Composites Part B: Engineering*, **94**, 109 (2016).
27. D. Askari, M.N. Ghasemi-Nejhad, *Journal of Sandwich Structures & Materials*, **22**(7), 2330 (2020).
28. M. Tapia, Y. Espinosa-Almeyda, R. Rodríguez-Ramos, J. A. Otero, *Appl. Sci.*, **11**(4), article 1867 (2021).
29. S. A. Banarouei, Master thesis, York University, Toronto, Ontario, Canada (2021).
30. Ts. V. Rangelov, Y. D. Stoynov, P. S. Dineva, *Journal of Theoretical and Applied Mechanics*, **52**, 335 (2022).
31. Ts. Rangelov, P. Dineva, *Springer Proceedings in Mathematics & Statistics*, **412**, 117 (2023).
32. S. Parvanova, P. Dineva, *ZAMM*, e202200445, (2023) https://doi.org/10.1002/zamm.202200445 (in press).
33. G. D. Manolis, P. S. Dineva, Ts. V. Rangelov, G. I. Dadoulis, *Engineering Analysis with Boundary Elements*, **153,** 251 (2023).
34. O. Volkersen, *Luftfahrtforschung*, **15,** 41 (1938).
35. D.A. Dillard, A.V. Pocius, Chapter 1, Fundamentals of stress transfer in bonded systems, D.A. Dillard (ed.), Adhes. Sci. Eng. Mech. Adhes., Elsevier Science B.V., Amsterdam, 2002.
36. H. L. Cox, *Br. J. Appl. Phys.*, **3** (3), 72 (1952).
37. X.-L. Gao, K. Li, *International Journal of Solids and Structures*, **42**, 1649 (2005).
38. K. K. Ang, K. S. Ahmed, *Composites: Part B*, **50**, 7 (2013).
39. S. I. Kundalwal, M. C. Ray, S. A. Meguid, *Journal of Applied Mechanics*, **81**, 091001-1 (2014).
40. Y.-G. Hu, Y. F. Li, J. Han, C. P. Hu, Zh. H. Chen, S. T. Gu, *Acta Mech*. **230**, 2771 (2019).
41. L. Gong, I. A. Kinloch, R. J. Young, I. Riaz, R. Jalil, K. S. Novoselov, *Advanced materials*, **22** (24), 2694 (2010).
42. L. Gong, Ph.D. Thesis, Faculty of Engineering and Physical Sciences, The University of Manchester, Manchester, UK, 2012.
43. C. Xu, T. Xue, W. Qiu, Y.Kang, *ACS Appl. Mater. Interfaces*, **8**, 27099 (2016).
44. F. Wang, PhD thesis, The University of Manchester, Faculty of Science and Engineering, 2017, UK.
45. W. Wang, Z. Li, A. J. Marsden, M. A. Bissett, R. J. Young, *2D Mater.*, **8**, article 035058 (2021).
46. M. Liu, Y. Zhuo, A. Sarycheva, Y. Gogotsi, M. A. Bissett, R. J. Young, I. A. Kinloch, *ACS Appl. Mater. Interfaces*, **14**, 10681 (2022).
47. https://fhart.files.wordpress.com/2009/04/sapromat.pdf, fig.3.13, Assessed 26.06.23
48. Th. Lacroix, B. Tiimans, R. Keunings, M. Desaeger, I. Verpoest, *Composites Science and Technology*, **43**, 379 (1992).
49. M. Dong, R. J. Young, D. J. Dunstan, D. G. Papageorgiou, *Composites Science and Technology*, **233**, article 109892 (2023).
50. T. Jiang, R. Huang, Y. Zhu, *Adv. Funct. Mater.*, **24**, 396 (2014).
51. M. S. Bronsgeest, N. Bendiab, S. Mathur, A. Kimouche, H. T. Johnson, J. Coraux, P. Pochet, *Nano Lett.*, **15** (8), 5098 (2015).
52. G. Guo, Y. Zhu, *Journal of Applied Mechanics*, **82** (3), 031005-1 (2015).
53. G. Wang, Z. Dai, L. Liu, H. Hu, Q. Dai, Zh. Zhang, *ACS Appl. Mater. Interfaces*, **8,** 22554 (2016).
54. L.-H. Shao, X. Qu, T. Wang, Z. Cui, Y. Liu, Y. Zhu, *J. Mech. Phys. Solids*, **173**, article 105218 (2023).
55. Y. Zhang, Z. Zhou, Z. Tan, *Symmetry*, **11**, 1437 (2019).
56. B. Zhao, Z-H. Lu, *Mechanics of Advanced Materials and Structures*, **16**, 130 (2009).
57. B. Zhao, Z.-H. Lu, Y.-N. Lu, *International Journal of Adhesion & Adhesives*, **49**, 115 (2014).
58. S.K. Gupta, D.K. Shukla, A. Bharti, in: Proc. 2017 International Conference on Advances in Mechanical, Industrial, Automation and Management Systems, 3-5 February 2017, Allahabad, India, 307.
59. E.A. Akpinar, K. Gültekin, S. Akpinar, H. Akbulut, A. Ozel, *Composites Part B*, **98**, 362 (2016).
60. P. Jojibabu, Y.X. Zhang, G. Prusty, *International Journal of Adhesion and Adhesives*, **96**, article 102454 (2020).
61. G. Liu, B. Ji, K.-C. Hwang, B. C. Khoo, *Composites Science and Technology*, **71,** 1190 (2011).
62. G. Wang, L. Liu, Zh. Zhang, *Composites Part A: Applied Science and Manufacturing*, **141**, article 106212, (2021).
63. J. Huang, J. Zhou, M. Liu, *JACS Au*, **2**(2), 280 (2022).
64. X. Lu, F. Detrez, J. Yvonnet, J. Bai, *Composites Science and Technology*, **213**, article 108943, (2021).
65. Ch. Androulidakis, E.N. Koukaras, J. Rahova, K. Sampathkumar, J. Parthenios, K. Papagelis, O. Frank, C. Galiotis, *Appl. Mater. Interfaces*, **9** (31), 26593 (2017).
66. I. Polyzos, M. Bianchi, L. Rizzi, E.N. Koukaras, J. Parthenios, K. Papagelis, R. Sordan, C. Galiotis, *Nanoscale*, **7**(30), 13033 (2015).
67. G. Anagnostopoulos, C. Androulidakis, E. N. Koukaras, G. Tsoukleri, I. Polyzos, J. Parthenios, K. Papagelis, C. Galiotis, *ACS Appl. Mater. Interfaces*, **7**, 4216 (2015).
68. F. Wang, S. Li, M. A. Bissett, I. A. Kinloch, Z. Li, R. J. Young, *2D Materials*, **7**(4), Article number 045022 (2020).